magnetochemistry

MDPI

Article

Structural Changes of Zn(II)bleomycin Complexes When Bound to DNA Hairpins Containing the 5′-GT-3′ and 5′-GC-3′ Binding Sites, Studied through NMR Spectroscopy

Shelby E. Follett [1], Sally A. Murray [1], Azure D. Ingersoll [1], Teresa M. Reilly [2] and Teresa E. Lehmann [1,*]

[1] Department of Chemistry, University of Wyoming, Laramie, WY 82071, USA; Shelby.follett@tolmar.com (S.E.F.); smurra15@uwyo.edu (S.A.M.); azureingersoll@gmail.com (A.D.I.)
[2] Department of Chemical Engineering, University of Wyoming, Laramie, WY 82017, USA; treilly2@uwyo.edu
* Correspondence: tlehmann@uwyo.edu; Tel.: +1-307-766-2772

Received: 9 November 2017; Accepted: 12 December 2017; Published: 27 December 2017

Abstract: We have previously investigated the diverse levels of disruption caused by Zn(II)BLMs with different C-termini to DNA hairpins containing 5′-GC-3′ and 5′-GT-3′ binding sites. The results of this investigation indicated that both the DNA-binding site and the bleomycin C-termini have an impact on the final conformation of the aforementioned hairpins in the drug-target complexes, as suggested by the different sets of intramolecular NOEs displayed by both oligonucleotides when bound to each Zn(II)BLM. The NMR signals elicited by ^{1}H nuclei in the oligonucleotide bases and sugar moieties were also affected differently (shifted upfield or downfield in various patterns) depending on the BLM C-termini and the binding site in the oligonucleotides. The overall conclusion derived from the precedent research is that the spatial conformation of target DNA segments in DNA-Zn(II)BLM complexes could be forged by interactions between drug and DNA that are guided by the DNA binding site and the BLM C-termini. The present study focuses on the structural alterations exhibited by Zn(II)bleomycin-A_2, -B_2, -A_5 and Zn(II)peplomycin molecules upon binding to the previously studied hairpins. Our main goal is to determine if different spatial conformations of the drugs in their DNA-bound forms are found in drug-DNA complexes that differ in the oligonucleotide binding site and BLM C-termini. Evidence that suggest that each Zn(II)bleomycin is structurally affected depending these two factors, as indicated by different sets of intramolecular NOE connectivities between drug protons and diverse patterns of shifting of their ^{1}H-NMR signals, is provided.

Keywords: DNA; NMR; pulmonary fibrosis; anticancer drug; structure-function

1. Introduction

Bleomycins (BLMs) compose a family of glycopeptide-derived antibiotics produced by *Streptomyces verticillus* [1]. BLMs have been used as chemotherapeutic agents in the clinical treatment of a wide spectrum of cancers, and their antitumor activity is generally proposed to be related to cleaving single-stranded or double-stranded DNA in carcinoma cells [2–4]. The overall structure of these agents can be thought of as containing four distinct regions (Figure 1): the metal binding domain (D1), which is responsible for metal binding [5,6], oxygen activation [5,7–9], and site-selective DNA cleavage [6,10]; the peptide linker (D2); the DNA binding domain (D3), containing a bithiazole moiety and the C-terminus, which provides the majority of the DNA binding affinity [11,12]; and the disaccharide moiety (D4), which influences metal ion binding [6,13–24] and is proposed to be a tumor-targeting unit [25].

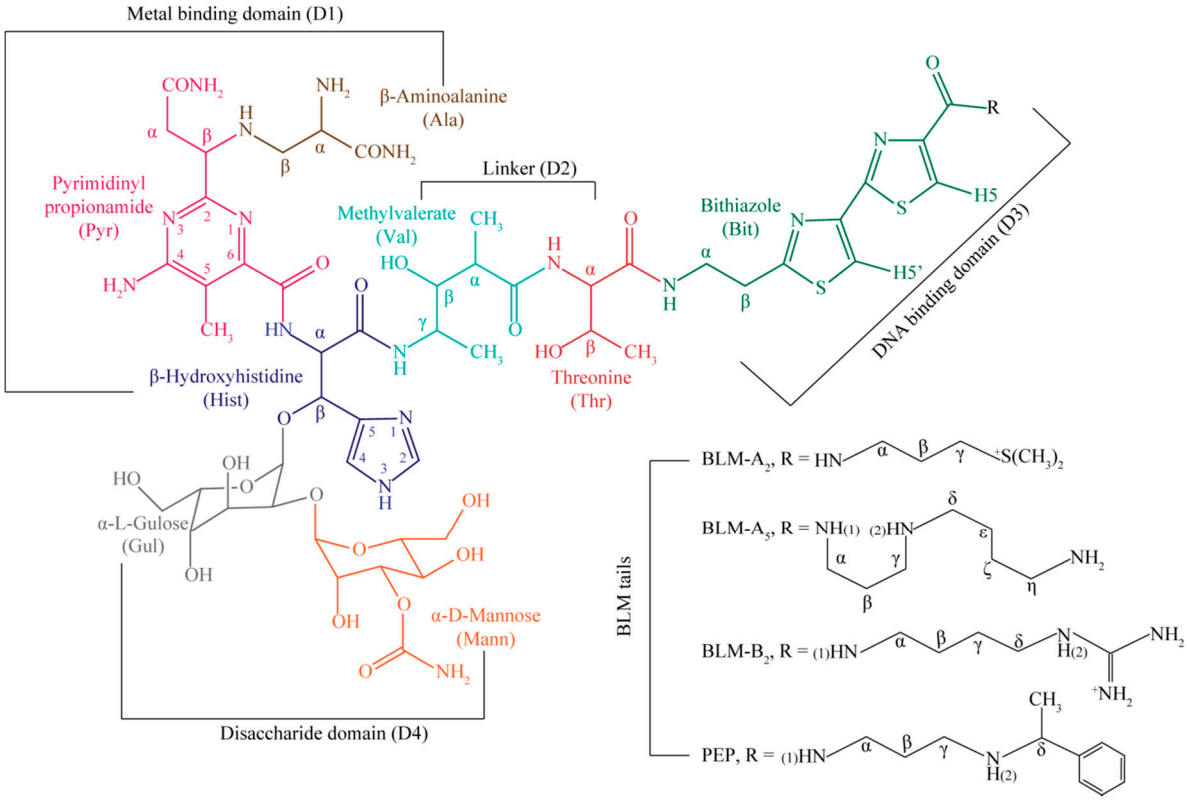

Figure 1. Structures BLM-A_2, -A_5, -B_2, and PEP showing the breakdown of the different domains, residues, and C-termini.

Although successful in the treatment of certain cancers, BLMs are associated with pulmonary toxicity, and extensive research is required to lower this risk to patients [16]. Biological studies performed by Raisfeld et al. [26–31] have linked the cause of pulmonary toxicity to the BLM C-termini (tails). Blenoxane, introduced in 1972, is the clinically used combination of BLMs, with the major components being BLM-A_2 and -B_2. Over 300 BLM analogs have since been developed with the hope of lowering the risk of pulmonary toxicity and achieving high levels of antitumor activity [32–34].

Research work on the interactions of various metallo-BLMs (MBLMs) with DNA fragments have generated abundant evidence indicating that the mode of binding of MBLMs to DNA is sensitive to various factors. These factors could include the DNA binding site, the DNA base sequence, the metal center bound to BLM, and the C-terminus of the drug. Different specific binding interactions between drug and target have been reported [35–44]; and various modes of binding of the bithiazole unit to different DNA fragments have been described including minor groove binding [35,37,45], and partial [40,42,43] or total [46] intercalation.

Most of the available research on MBLMs bound to DNA fragments focus on the structure of the full drug-target complex, and briefly mention how the MBLM molecule is affected upon binding to DNA. Manderville et al. showed that there are differences between the structural changes of Zn(II)BLM-A_2 and Zn(II)BLM-A_5 upon complexation with a DNA fragment with a 5′-GC-3′ binding site, and that the structure of Zn(II)BLM-A_5 was more disrupted than that of Zn(II)BLM-A_2 after binding [37]. Vanderwall et al. showed that when HOO-Co(III)BLM-A_2 was bound to DNA fragments with either the 5′-GC-3′ and 5′-GT-3′ binding sites there were little differences in the structural changes to the Zn(II)BLM [38]. Some of the available studies have briefly examined the influence DNA has on the MBLM structure, focusing almost exclusively on the bithiazole (Bit) and the β-hydroxyhistidine (Hist) moieties in BLM [35–39,47,48]. Additionally, the BLMs used in these studies are limited, with the majority using MBLM-A_2 [35–43,47], and some investigating MBLM-A_5 [37], MBLM-B_2 [46]

and metallo-PEP [49]. Although the precedent work has provided the scientific community with important information regarding DNA-MBLM interactions, the multiplicity of DNA fragments, metal centers, and BLM C-termini used makes it difficult to generalize the findings.

We have previously performed two studies to determine the significance of various factors that could influence the final conformation of target DNA segments in Zn(II)BLM-DNA triads, using DNA hairpins of sequences 5′-AGCCTTTTGGCCT-3′ (OL_1) containing a 5′-GC-3′ binding site [50] and 5′-CCAGTATTTTTACTGG-3′ (OL_2) containing 5′-GT-3′ binding site [51]. The first study entailed investigating the effect that the BLM tails have on the binding of Zn(II)BLMs to a DNA hairpin of containing the 5′-GC-3′ binding site. The second study tested the role of the DNA binding site (5′-GC-3′ or 5′-GT-3′) in the relative spatial arrangement of the Zn(II)BLM-target complexes. The results of this work indicated that both the DNA-binding site and the bleomycin C-termini have an impact on the final conformation of the aforementioned hairpins in the drug-target complex, as suggested by the different sets of intramolecular NOEs displayed by both oligonucleotide (OLs) when bound to each Zn(II)BLM. The NMR signals elicited by ^{1}H nuclei in the OL bases and sugar moieties were also affected differently (shifted upfield or downfield in various patterns) depending on the BLM C-termini and the binding site in the OLs. The work presented herein has the goal of determining if the BLM chemical structure and the DNA binding site affect the conformation of Zn(II)BLM molecules in their OL1- and OL2-bound states. These studies all involve a Zn^{2+} metal center. Zn(II)BLMs maintain the same ligands that participate in chelation as Fe(II)BLMs [14,15,20–23] which, in the presence of oxygen, becomes HOO-Fe(III)BLM, the activated form of the MBLM proposed to cleave DNA in vivo. Due to the potential for DNA cleavage and paramagnetic nature of MBLMs containing the Fe(III) ion, Zn(II)BLMs are, in our opinion, the best diamagnetic inactive models for Fe(II)BLM, which is the next MBLM to be studied in our laboratory to determine the relevance of the metal center in MBLM-DNA interactions. The DNA base sequences were selected to be very similar to those used on studies of MBLMs bound to various DNA fragments with the aim of comparing our results to those of other researchers on the field. Due to the short lengths of various oligonucleotide previously reported in the available literature, and their self-complementarity, we decided to use DNA hairpins in order to guarantee that the BLM-binding site was located in a double-stranded region of the DNA segment, while keeping the OL at minimum complexity for the sake of NMR data analysis. The selected hairpins still contain the important inter-strand interactions found in double-stranded DNA, and therefore are a valid test models. In our previous work on the conformational changes exhibited by OL1 [50] and OL2 [51] in the presence of various Zn(II)BLMs we confirmed that the free OLs display sets of inter- and intra-strand NOEs that indicate normal double-stranded structures crowned by loops. We present here the structural changes the Zn(II)BLM molecules suffer upon binding to these hairpins.

2. Results

The ^{1}H-NMR signals elicited by free Zn(II)BLM-A_2, -A_5, -B_2, and Zn(II)PEP were assigned using COSY, TOCSY, and NOESY spectra acquired in H_2O at 5 °C. These assignments are collected in Supplementary Table S1. The NOESY spectra of these Zn(II)BLMs bound to OL_1 and OL_2 (Supplementary Figures S1–S4) acquired in H_2O at 5 °C previously examined [50,51] were analyzed this time to identify the signals generated by the bound Zn(II)BLMs, and investigate the effects that OL complexation has on the conformation of each Zn(II)BLMs. The spectra acquired for all Zn(II)BLM-DNA triads in D_2O at both 5 °C and 25 °C and in H_2O at 25 °C [50,51] were also used for confirmation of some of the peak assignments. The work described herein looks at the structural changes of the entire Zn(II)BLM molecule upon binding to the OLs, and allows for comparability between the different Zn(II)BLMs studied and the preferential binding sites in DNA.

Our previous studies on the Zn(II)BLM-DNA triads [50,51] show that Zn(II)BLMs are bound to both OLs through the analysis of one-dimensional (1D) ^{1}H-NMR spectra at both 5 °C in H_2O and 25 °C in D_2O. The proton signals in the imino region for the OLs are significantly affected in both studies, exhibiting downfield shifting and broadening for both OLs. The bithiazole (Bit) and β-hydroxyhistidine

(Hist) ring protons of the Zn(II)BLMs also shift and broaden upon binding, and are essential when investigating the potential binding mode of the drugs to DNA [50,51]. As previously reported and shown in Table 1, the Bit aromatic signals in each Zn(II)BLM exhibit changes upon complexation to the OL1. In all cases, there is broadening and shifting of these signals for each Zn(II)BLM-OL1 triad indicating binding to OL1. However, there are differences in their behavior depending on the Zn(II)BLM bound. The Zn(II)BLM-A_5-OL1 triad exhibits large downfield shifting for the CH5 and CH5′ protons, with the -A_2-OL1, -B_2-OL1, and PEP-OL1 triads displaying upfield shifts in decreasing order, respectively [50]. Upon complexation of Zn(II)BLM-A_2 and Z n(II)PEP to OL2, the Bit ring protons also experience broadening and shifting. Examination of the Δδ values shown in Table 1 indicates that the Bit signals have a greater upfield shift in OL_2-bound Zn(II)PEP than in the Zn(II)BLM-A_2-OL2 triad [51]. This trend is opposite to that exhibited by the same signals in the OL1 triads.

Table 1. Chemical shift differences (Δδ) between free and OL-bound Zn(II)BLM for spectra acquired in H_2O at 5 °C.

Residue	OL_1 Zn(II)BLM-A_2	OL_2 Zn(II)BLM-A_2	OL_1 Zn(II)PEP	OL_2 Zn(II)PEP	OL_1 Zn(II)BLM-B_2	OL_1 Zn(II)BLM-A_5
Val $C^{\alpha}H$	0.17 [a]	−0.07	0.21	−0.06	0.21	0.33
Val $C^{\beta}H$	−0.03	−0.06	−0.03	−0.29	−0.03	−0.07
Val $C^{\gamma}H$	−0.02	−0.06	−0.02	−0.08	−0.02	−0.03
Val $C^{\alpha}CH_3$	0.03	0.00	0.04	−0.04	0.03	0.02
Val $C^{\gamma}CH_3$	−0.01	−0.02	−0.01	0.19	−0.01	−0.01
Val NH	0.05	−0.10	0.05	[b] -	0.08	0.09
Thr $C^{\alpha}H$	−0.02	−0.05	−0.03	−0.04	−0.04	−0.05
Thr $C^{\beta}H$	−0.03	−0.05	−0.04	−0.05	−0.04	−0.09
Thr CH_3	−0.01	−0.02	−0.02	−0.01	−0.02	−0.04
Thr NH	0.15	−0.02	0.19	-	0.18	0.28
Bit $C^{\alpha}H_2$	0.05	0.08	0.06	0.12	0.07	0.10
Bit $C^{\beta}H_2$	0.02	0.05	0.03	0.09	0.02	0.05
[c] Bit C5′H	0.19	0.19	0.37	0.07	0.09	−0.19
[c] Bit C5H	-	-	0.36	-		−0.37
Bit NH	−0.02	−0.03	−0.03	0.01	−0.04	−0.05
Ala $C^{\alpha}H$	−0.01	0.00	−0.01	0.04	−0.01	0.00
Ala $C^{\beta}H_{2b}$	0.00	−0.01	−0.01	−0.05	−0.01	0.00
Ala NH	-	-	0.05	-	-	-
Ala NH_{2a}	0.00	0.01	−0.01	−0.04	−0.01	−0.01
Ala $CONH_{2a}$	−0.01	−0.01	−0.02	−0.14	−0.01	0.00
Ala $CONH_{2b}$	0.00	0.02	0.00	0.04	0.00	0.02
Pyr NH_2	−0.03	−0.04	−0.04	−0.05	−0.03	−0.02
Hist C2H	−0.05	−0.23	−0.01	−0.11	−0.03	−0.03
Hist C4H	−0.02	−0.04	−0.01	−0.03	−0.03	−0.04
Hist $C^{\alpha}H$	0.00	0.06	−0.03	0.01	0.00	−0.01
Hist $C^{\beta}H$	0.00	0.05	−0.01	−0.01	−0.01	0.00
Mann C1H	0.03	0.07	0.01	-	0.01	-
Mann C6H	-	-	-	−0.06	-	-
Mann C6H′	-	-	-	−0.04	-	-
Mann NH_{2a}	−0.01	−0.07	−0.01	−0.07	−0.01	−0.01
Gul C2H	0.00	−0.01	0.01	−0.04	0.01	0.00
[d] A_2 $C^{\beta}H_2$	0.01	0.06				
A_2 $C^{\gamma}H_2$	0.05	0.16				
A_2 NH	0.09	0.23				
PEP $C^{\alpha}H_2$			0.03	0.13		
PEP $C^{\gamma}H_{2a}$			−0.01	0.04		
PEP $C^{\delta}H$			0.01	0.04		
PEP NH (2)			0.10	-		
B_2 $C^{\alpha}H_{2a}$					0.05	
B_2 $C^{\gamma}H_{2a}$					−0.04	
B_2 NH (1)					0.13	
A_5 $C^{\alpha}H_2$						0.08
A_5 NH_{2a}						0.24

[a] Calculated as [(Free Zn(II)BLM)–(Bound Zn(II)BLM)]; [b] Unassignable; [c] Reported in [50,51]; [d] Red labels indicate tail protons for each Zn(II)BLM.

Table 1 also displays the Δδ values between the free and OL-bound forms of Zn(II)BLM for protons in other moieties of the BLM molecules that experience significant shifts ($\Delta\delta \geq 0.04$ ppm) upon complexation to OL1 and OL2. It is clear from this table that, when bound to the OLs, each Zn(II)BLM experiences a wide range of significant shifts from their original positions in the free forms. Additionally both upfield and downfield shifts are observed. For some protons, the preferential binding site (5′-GC-3′ (OL_1) vs. 5′-GT-3′ (OL_2)) influences the direction and magnitude of the shift (Table 1, columns 2–5). Another interesting result is that some of the signals experience a significant shift for only one of the triads. Additionally, the Methylvalerate (Val) $C^{\alpha}H$ and the $C^{\alpha}H_2$ aliphatic protons in Bit exhibit significant shifts for all triads. Most of the available structural work on MBLM triads formed with DNA fragments focus on the Bit and Hist moieties. Our results show that most of the Bit moiety protons shift upfield, with the exception of the Bit NH proton, for all complexes. However, the degree and direction of this shifting is dependent upon the triad. The Hist ring protons, C2H and C4H, move downfield for all complexes with different degrees of shifting. These shifts show that although all Zn(II)BLMs studied share the same D1, D2, and D4, each of them is impacted differently, in terms of Δδ, based on the chemical structure of the C-terminus and the binding site in the OLs.

Using schematic diagrams, we illustrate which Zn(II)BLM protons experience significant shifts upon binding to OL_1 and OL_2, based on the results shown in Table 1. Figure 2 shows the Zn(II)BLM protons that experience significant shifts (red circles) in the OL_1 triads. Figure 3 shows the Zn(II)BLM protons that experience significant shifts (green circles) in the OL_2 triads. The protons circled in purple were assigned in the free form of the Zn(II)BLMs, but could not be assigned in their OL-bound forms. Figures 2 and 3 schematically show that both, the BLM tail and the binding site in DNA have an effect on the magnetic and/or chemical environment experienced by some protons in the Zn(II)BLMs. It is important to indicate that the NMR signals of most of the Zn(II)BLM sugar protons could not be assigned due to significant overlap with the signals coming from the sugar moieties in OL_1 and OL_2.

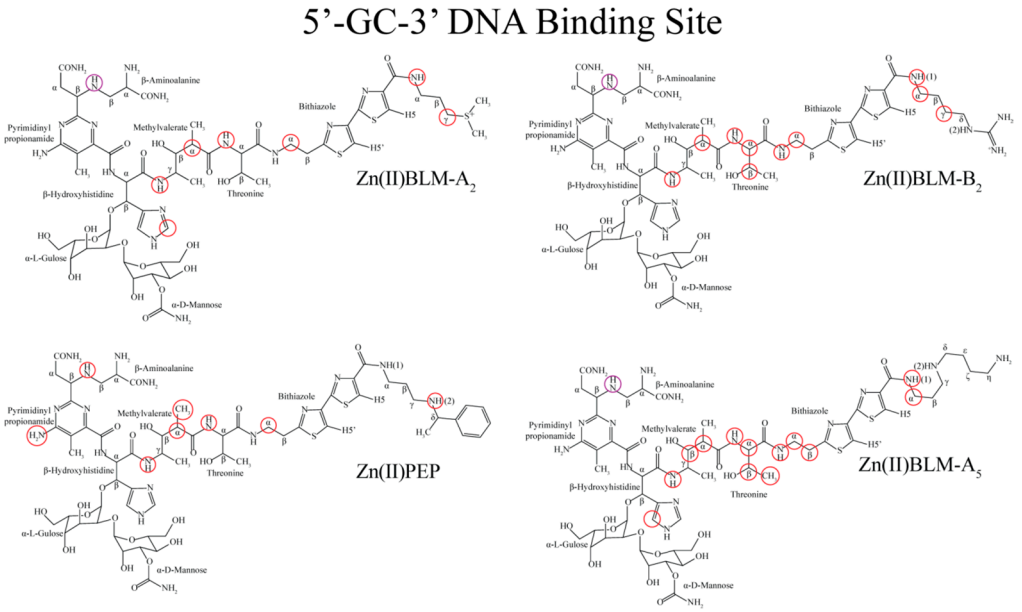

Figure 2. Protons exhibiting significant shifts in their OL_1-bound forms. (red circles) and protons that could not be assigned in the bound forms (purple circles) for spectra acquired in H_2O at 5 °C.

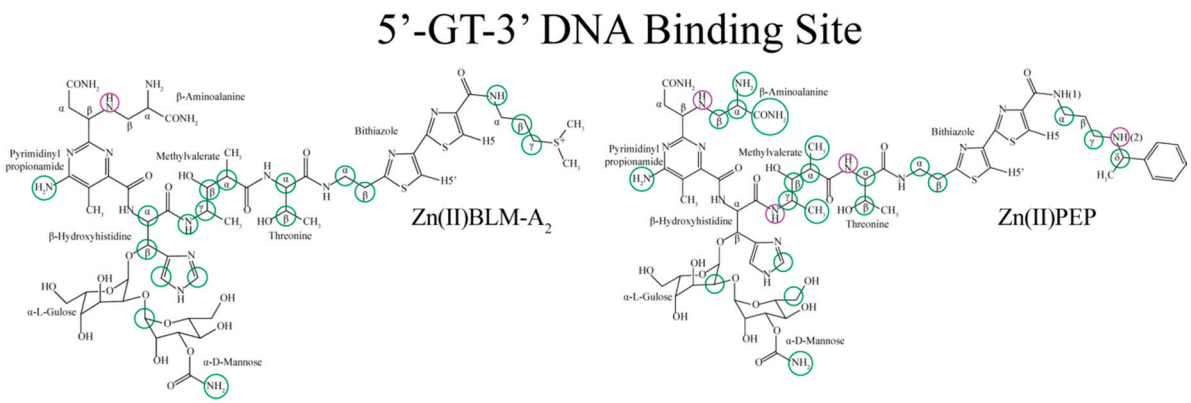

Figure 3. Protons exhibiting significant shifts in their OL_2-bound forms (green circles) and protons that could not be assigned in the bound forms (purple circles) for spectra acquired in H_2O at 5 °C.

Analysis of Figure 2 shows that in the OL_1 triads, Zn(II)BLM-A_2 and Zn(II)PEP are the least affected Zn(II)BLMs after binding, compared to Zn(II)BLM-B_2 and -A_5. In general terms, the significant shifts are contained within D2 and D3. The OL_1 triads with Zn(II)BLM-A_2 and -A_5 experience significant downfield shifts of the Hist C2H and C4H protons, respectively. The Ala NH protons is affected in all OL_1 triads, however, this signal in the bound Zn(II)BLMs could only be assigned in the Zn(II)PEP-OL_1 complex. Additionally, one of the Pyr NH_2 protons experiences significant downfield shifts in the Zn(II)PEP-OL_1 triad and in both OL_2 triads (Figure 3).

Comparison of Figures 2 and 3 shows that when the Zn(II)BLMs are complexed with the same OL, the chemical and/or magnetic environment of some protons vary based on the C-termini in BLM. However, when the same Zn(II)BLM is bound to both OLs, OL_2 has a greater effect on the new environments of the protons in that Zn(II)BLMs than OL_1. Specifically, for Zn(II)BLM-A_2 and Zn(II)PEP complexed with OL_2, many additional protons experience significant shifts, and the affected protons are no longer limited to D2 and D3. For both OL_2 triads, many of the D1 protons experience significant shifts. Additionally, the Hist and Ala moieties are greatly shifted in Zn(II)BLM-A_2 and Zn(II)PEP, respectively in the OL_2 triads. These results indicate that the metal binding domain experiences different environments upon complexation dependent upon the chemical structure of the BLM tail and the BLM-binding site in the OLs.

The spectra acquired for the Zn(II)BLM-DNA triads exhibit signals for the three ligands to the metal center containing protons: Ala NH, Ala NH_2, and Mann NH_2. The Ala NH proton signal could not be identified for the OL-bound forms of the Zn(II)BLM, except in the Zn(II)PEP-OL_1 complex. This result indicates that this ligand is somehow affected by the binding to the OLs, and exhibits a significant $\Delta\delta$ in Zn(II)PEP upon binding to OL_1. Furthermore for both of the OL_2 triads under study, one of the Mann NH_2 protons shows a significant $\Delta\delta$ after binding to OL_2, in addition to both protons in Ala NH_2 for the Zn(II)PEP-OL_2 triad. The Hist N1 and NH (deprotonated upon metal coordination) ligands do not generate ^{1}H-NMR signals, however, the Hist $C^{\alpha}H$ and Hist C2H protons are in close proximity to these ligands. The Hist C2H proton displays significant $\Delta\delta$s for both OL_2 triads, and the Zn(II)BLM-A_2-OL_1 complex. Additionally, the Hist $C^{\alpha}H$ proton is significantly shifted for the Zn(II)BLM-A_2-OL_2 triad. These results suggest that there are diverse possibilities for the magnetic and/or chemical environments experienced by the metal coordination cage dependent upon the BLM C-terminus and the DNA binding site.

We continued our analysis of DNA-bound Zn(II)BLMs by looking at how the intra-residue and inter-residue intramolecular NOEs for each of them are affected upon binding to the OLs. Figure 4 shows the inter-residue intramolecular NOEs for each Zn(II)BLM before complexation with the OLs for samples in H_2O at 5 °C (these NOEs are collected in: Zn(II)BLM-A_2, Supplementary Table S2; Zn(II)PEP, Supplementary Table S4; Zn(II)BLM-B_2, Supplementary Table S6; and Zn(II)BLM-A_5, Supplementary Table S8). This figure shows how each Zn(II)BLM is folded with complex through-space

connections, however, each of them is different regarding their native conformations. Both Zn(II)PEP and Zn(II)BLM-A_2 have inter-residue intramolecular NOEs connecting the BLM tails to residues in D1, D2, and D4, indicating a more compact folded structure than Zn(II)BLM-B_2 and -A_5. Also indicative of a folded structure are the inter-residue intramolecular NOEs between D1 and D2, as well as between D4 and D2 observed for all Zn(II)BLMs.

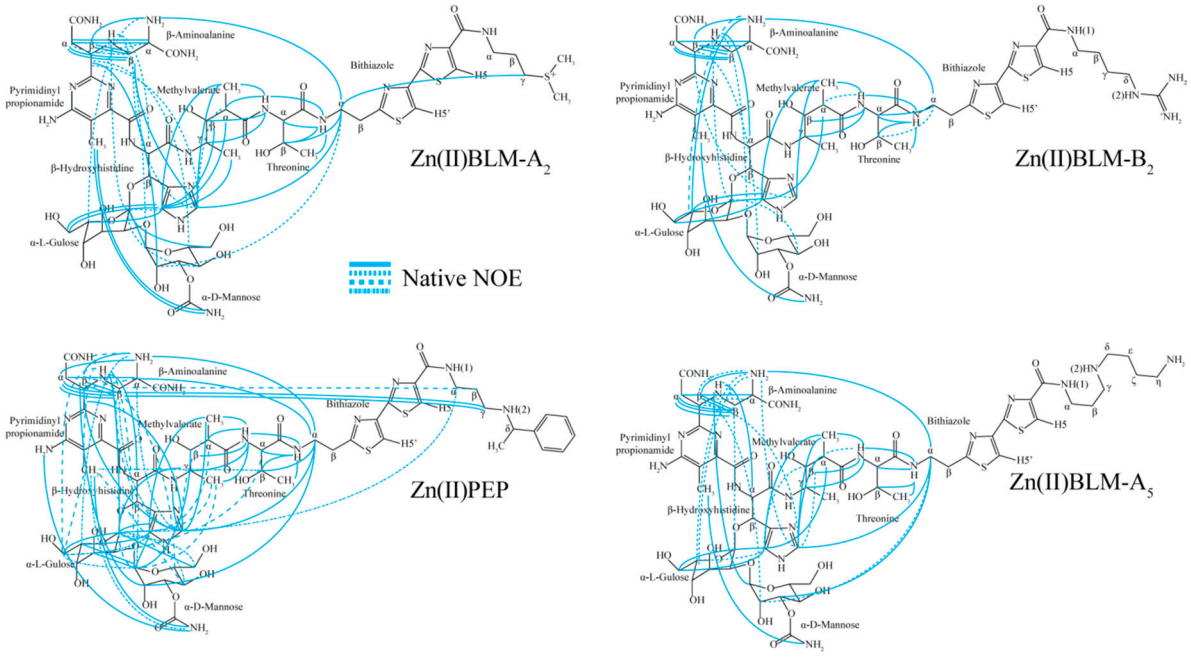

Figure 4. Inter-residue intramolecular NOEs for each Zn(II)BLM under study in their native forms. Data taken from spectra acquired in H_2O at 5 °C for Zn^{2+}:BLM samples in a 1:1 molar ratio. Dashed and continuous lines all represent NOE connectivities, they are used to avoid confusion in busy sectors of the figure.

Some of the inter-residue intramolecular NOEs present in the free Zn(II)BLMs (native NOEs) are also detected in their OL-bound forms. These NOEs, together with inter-residue intramolecular NOEs that arise in the Zn(II)BLMs upon binding to the OLs (new NOEs), are presented in Figures 5 and 6 for Zn(II)BLMs bound to OL_1 and OL_2, respectively. Supplementary Tables S2, S4, S6, and S8 show these NOEs for each OL-bound Zn(II)BLM. Supplementary Tables S3, S5, S7, and S9 display the intra-residue intramolecular NOEs for each free and OL-bound Zn(II)BLM.

Examination of these tables and Figures 4–6 leads to some interesting facts regarding the differences in conformation of the Zn(II)BLMs between their native and OL-bound forms. Comparison of Figures 4 and 5 shows that Zn(II)BLM-A_5 and Zn(II)BLM-B_2 lose more of their native NOEs than Zn(II)BLM-A_2 and Zn(II)PEP after complexation with OL_1. This result suggest that there is a greater degree of unfolding of these Zn(II)BLMs in their OL_1-bound forms. A multitude of new NOEs are connecting D1 and D2 protons in the OL_1-bound Zn(II)BLMs, and suggest refolding of the Zn(II)BLMs around D2. One of these NOEs connects Hist C2H to Threonine (Thr) CH_3, which interestingly is present for all OL_1 triads, but neither of the OL_2 triads (Figures 5 and 6). Comparison of Figures 5 and 6 shows many substantial differences in the conformations of the Zn(II)BLMs when bound to the two OLs. This fact based on the number and differences in the native and new NOEs that each bound Zn(II)BLM displays. Some of the new NOEs in the two OL_2 triads are connecting D1 and D3, which is also observed in the Zn(II)BLM-A_5-OL_1 complex. Examination of Zn(II)PEP bound to both OLs shows that there is a greater reduction in the number of native NOEs when this Zn(II)BLM is complexed with OL_2, which is significant around D1. In the free Zn(II)BLMs there is a multitude of NOEs connecting Ala protons with D4 and Hist protons. These NOEs suggest that D1 and D4 are involved in metal ion

coordination. The limited number of these connections that remain after the Zn(II)BLMs bind to the OLs provide evidence suggesting that this segment has rearranged upon complexation to the OLs and each Zn(II)BLM-OL triad displays different conformations for it.

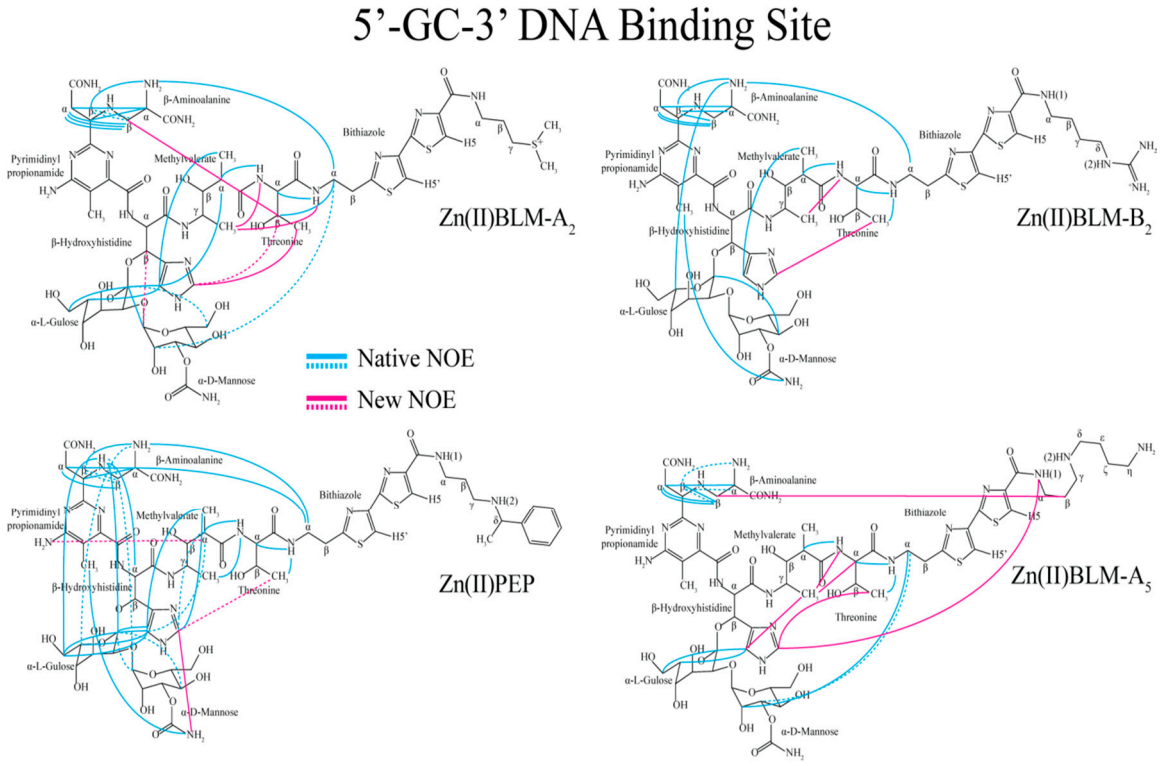

Figure 5. Inter-residue intramolecular NOEs for each OL_1-bound Zn(II)BLMs. Samples of Zn(II)BLMs:OL_1 are in a 1:1 molar ratio in H_2O at 5 °C. Dashed and continuous lines all represent NOE connectivities, they are used to avoid confusion in busy sectors of the figure.

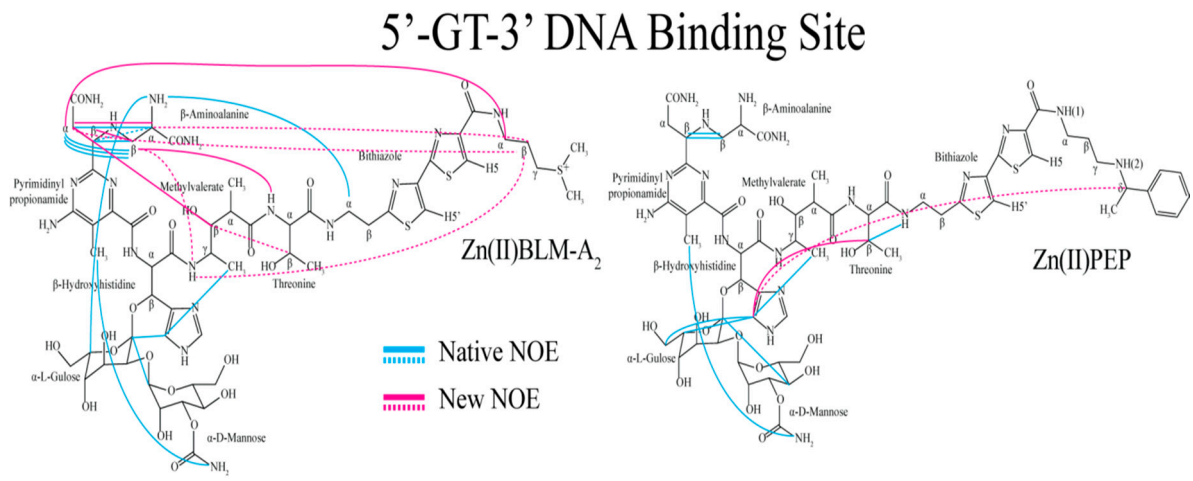

Figure 6. Inter-residue intramolecular NOEs for each OL_2-bound Zn(II)BLM for samples of Zn(II)BLM:OL_2 in a 1:1 molar ratio in H_2O at 5 °C. Dashed and continuous lines all represent NOE connectivities, they are used to avoid confusion in busy sectors of the figure.

The Pyr and Hist moieties show NOEs with the D4 in the free Zn(II)BLMs. Upon complexation to the OLs, changes to these NOEs appear that are diverse for each triad. This fact indicates that there is possible rearrangement of the metal coordination cage upon triad formation. The aforementioned

results can be summarized to argue in favor of molecular rearrangement of the Zn(II)BLMs after triad formation. The NOE connections (native and new) present in the triads indicate that OL complexation impact the folding of the Zn(II)BLMs diversely depending on both the preferential binding site in the DNA fragment and the chemical structure of the BLM tail.

Table 2 displays a summary of the changes exhibited by the Zn(II)BLMs upon binding to the OLs. Examination of this table indicates that there is a significant difference between the conformations of Zn(II)PEP when complexed with OL_1 and OL_2. Only 44% of the native inter-residue intramolecular NOEs remain when bound to OL_1, but that percentage decreases to 13% when bound to OL_2. This trend is not displayed by bound Zn(II)BLM-A_2, the percentages being 43% for OL_1 and 38% for OL_2. The finding that there is a difference between the parameters shown in Table 1 when Zn(II)BLMs are bound to different OLs are compared indicates that the DNA-binding site has an impact on the final conformation of the drug. When comparing OL_2 triads, it can be seen that Zn(II)PEP conserves a significantly smaller amount of connections than Zn(II)BLM-A_2, with the percentages being 13% and 38%, respectively. This result could be interpreted to suggest that the chemical structure of the BLM-tail has an effect on the final conformation of the bound drug.

Table 2. Comparison of the overall changes in significant signal shifts and native and new NOEs displayed by the Zn(II)BLMs after binding to the indicated OL.

	OL_1 Triads				**OL_2 Triads**	
	A_2	**PEP**	**B_2**	**A_5**	**A_2**	**PEP**
% Overall native NOEs detected	51	48	56	50	43	26
Number of new intra-residue NOEs	3	2	2	1	0	0
% Native inter-residue NOEs	43	44	42	38	38	13
Number of new inter-residue NOES	6	3	2	6	10	2
Number of intermolecular NOEs	1	3	0	0	4	8
Number of significantly shifted BLM residues	8	8	11	14	19	25

3. Discussion

We have previously investigated the diverse levels of disruption caused by Zn(II)BLMs with different C-termini to DNA hairpins containing 5′-GC-3′ (OL1) [50] and 5′-GT-3′ (OL2) [51] binding sites. The results of this investigation indicated that, in the presence of different Zn(II)BLMs, both OLs display different patterns of intramolecular NOE connectivities and ^{1}H-NMR signal shifting suggesting that they exhibit different solution conformations in their Zn(II)BLM-bound forms. The overall conclusion derived from the precedent research is that the spatial conformation of target DNA segments in DNA-Zn(II)BLM complexes could be forged by interactions between drug and DNA, that are guided by the DNA binding site and the BLM C-termini.

The information presented herein is focused on the structural disturbances displayed by the same four Zn(II)BLMs that take place after these molecules bind to the aforementioned OLs. We have found that globally, OL_2 causes a greater degree of disturbance to the Zn(II)BLM structures than OL_1, just as the structure of OL_2 was more disturbed upon binding to the Zn(II)BLMs than that of OL_1 [50,51]. Additionally when complexed with OL_1, the shifts of the protons and the inter-residue NOE network of Zn(II)PEP were affected the least followed by Zn(II)BLM-A_2 and -B_2, with Zn(II)BLM-A_5 being the most affected; which is in direct correlation to the effects of these Zn(II)BLMs on the OL_1 structure [50]. We separate our discussion of the structural changes observed in the different Zn(II)BLMs based on the BLM domains indicated in Figure 1.

3.1. Bithiazole (D3)

The DNA-binding domain (D3) in MBLMs has been the focal point of the investigation of many MBLM-DNA triads, due to its ability to closely interact with the DNA bases. The interactions between the Bit moiety and various DNA fragments have been interpreted to highlight a particular binding

mode of different MBLMs to DNA [36]. Examination of Figure 4 shows that all Zn(II)BLMs described herein exhibit NOEs connecting the Bit $C^{\alpha}H_2$ and NH protons to other residues in the metal complex before DNA binding occurs. After triad formation, the number of inter-residue intramolecular NOEs displayed by these protons is notably reduced, with the greatest effect occurring in the Zn(II)BLM-OL_2 triads, suggesting that the DNA-binding site has an effect on the location of D3 relative to the rest of the BLM molecule. The NOE networks for the Zn(II)BLM-A_2, -B_2, and Zn(II)PEP in the OL_1 triads show that the Bit $C^{\alpha}H_2$ protons remain in close contact with the Ala NH_2 protons, one of the ligands involved in metal ion coordination. Meanwhile, Bit $C^{\alpha}H_2$ protons are in close contact with a couple of the sugar protons in the Mann moiety for the Zn(II)BLM-A_5-OL_1 complex, suggesting a different conformation of the linker. The Mann NH_2 protons are involved in metal ion coordination as well, and thus the Bit $C^{\alpha}H_2$ protons are in a different location with respect to the coordinated metal center in this triad. These results suggest that the relative locations of D1 and D3 change upon triad formation, depending on the C-terminus in BLM.

In its OL_1 triad, the Bit $C^{\alpha}H_2$ in Zn(II)PEP exhibit NOEs with Ala NH_2 and Pyr $C^{\alpha}H_2$, while the Bit NH shows NOEs with two Thr protons. The aforementioned Bit $C^{\alpha}H_2$ NOEs have disappeared in the OL_2 triad for this Zn(II)BLM, and the Bit NH to Thr NOEs are different. Previously we have shown that the binding affinity of Zn(II)PEP is greater for OL_2 than for OL_1 [51] and thus the binding interaction of the Bit moiety is likely different when involving the two preferential binding sites. For both Zn(II)BLM-A_2 triads, the Bit $C^{\alpha}H_2$ protons are in close contact with the Ala NH_2 protons. On the other hand the NOEs between Bit NH and Thr $C^{\alpha}H$ and $C^{\beta}H$, and Val $C^{\gamma}CH_3$ in the OL_1 triad are missing in the OL_2 triad for this Zn(II)BLM. Based on these results we can propose that the conformation of the linker in BLM is also affected by the DNA-binding site.

3.2. *C-termini* (*D3*)

Before complexation to the OLs (Figure 4), Zn(II)BLM-A_2 displays one inter-residue intramolecular NOE between Bit $C^{\alpha}H_2$ and the $C^{\gamma}H_2$ protons of the tail, and Zn(II)PEP has multiple NOE connections connecting the metal binding domain and the tail. On the other hand, Zn(II)BLM-B_2 and -A_5 do not exhibit any inter-residue intramolecular NOEs involving tail protons. These results seem to indicate a high level of flexibility in solution for this region of the free Zn(II)BLM molecules. Upon complexation with OL_1, the inter-residue intramolecular connections of the tails in Zn(II)PEP and Zn(II)BLM-A_2 are no longer detected. However, there are two new NOEs for Zn(II)BLM-A_5 with the metal binding domain (Figure 5). Complexation of Zn(II)BLM-A_2 and Zn(II)PEP to OL_2 (Figure 6) leads to multiple NOEs involving the tail protons in the A_2 triad, and one of these NOEs for the PEP triad. These results suggest that after the Zn(II)BLMs bind OL_1 and OL_2, the BLM tails are positioned differently with respect to the rest of the BLM moieties depending on the OL available and possibly their chemical structures. In our previous studies involving the conformational changes of OL_1 and OL_2 in the presence of the Zn(II)BLMs discussed herein [50,51], we proposed that the conformation of each Zn(II)BLM-bound OL will be affected depending on the C-terminus of each Zn(II)BLM and the binding site present in each OL (5′-GC-3′ vs. 5′-GT-3′). If the tail location in bound Zn(II)BLMs is a consequence of the final conformation of the corresponding OL, or the interactions of D3 with the DNA helix remains to be demonstrated.

3.3. *Linker* (*D2*)

The linker region has previously been identified to contribute to the efficiency of DNA cleavage by bleomycin, and is necessary for promoting a compact structure [52]. In the present study, we have shown that the linker region is greatly affected upon binding to both DNA hairpins. For all OL-bound Zn(II)BLMs, the protons in the linker region exhibit some of the most significant Δδs calculated (Table 1), with Zn(II)BLMs bound to OL_2 showing the greater effect on their chemical shifts. As it can be seen in Table 1, the Val $C^{\alpha}H$ proton displays upfield shifts for Zn(II)BLMs bound to OL_1. On the other hand the Δδs calculated for this proton for Zn(II)BLMs bound to OL_2 show downfield

shifting. The Val $C^{\beta}H$ and $C^{\gamma}H$ protons all shift downfield upon OL complexation, with the most significant shifts observed for drugs complexed with OL_2. Significant changes in the chemical shifts of the linker protons are expected upon OL complexation, due to the different roles attributed to D1 (metal binding) and D3 (DNA binding) in the presence of DNA. However, it is clear from the results presented herein that the chemical and/or magnetic environment experienced by these protons depends on the C-terminus of each drug and the binding site available. Previous studies have reported that the Val $C^{\alpha}H$ has a significant upfield shift for MBLMs when complexed with DNA, and it is most likely indicative of a structural change in the BLM molecule rather than being involved in DNA base pair stacking [36,53]. Although, studies involving HOO-Co(III)BLM-A_2 complexed to DNA fragments containing 5′-GC-3′ and 5′-GT-3′ binding sites report a significant downfield shift for this proton [38,41]. It is possible that the metal center (Co(III) vs. Zn(II)) also has an effect on the chemical and/or magnetic environment this proton is exposed to after DNA binding.

The network of inter-residue intramolecular NOEs displayed by the free Zn(II)BLMs for the linker region is also modified upon binding. Only a few of the native NOEs are detected in the OL-bound forms of most Zn(II)BLMs, with OL_1-bound Zn(II)PEP exhibiting the highest number of these NOEs. Simplification of the NOE network of the linker is expected if the Zn(II)BLM molecules refold upon DNA complexation. Our results suggest that the Zn(II)BLM molecule adopts a more open conformation as a consequence of DNA binding. As shown in Figures 5 and 6, new NOEs are detected for the OL-bound forms of the Zn(II)BLMs. For the linker region, the number of native NOEs conserved and the new NOEs detected for each OL_1-bound Zn(II)BLM are different. The same conclusion regarding these factors can be drawn from a comparison of Zn(II)BLM-A_2 and Zn(II)PEP bound to OL_1 and OL_2. NOEs connecting the linker protons to protons in other BLM residues have been detected in previous studies of MBLM-DNA triads, and were interpreted to indicate that the MBLM molecule is folded compactly [35,37,54]. Our results show that the folding of OL-bound Zn(II)BLMs seem to depend on the C-termini in BLM and the DNA-binding site.

3.4. Metal Binding Domain (D1)

The metal binding domain is of great interest due to its chemical interaction with DNA during DNA cleavage by MBLMs [9]. Examination of Table 1 shows interesting differences between OL_1- and OL_2- bound Zn(II)BLMs. OL_1-bound Zn(II)BLM-A_2, Zn(II)PEP, and Zn(II)BLM-A_5 display significant downfield shifts of the Hist C2H, Pyr NH_2 and Ala NH, and Hist C4H, respectively. When the same Zn(II)BLMs are bound to OL_2, the Hist C2H downfield shift increases, and other protons in the Hist, Pyr, and Mann moieties show significant shifts for Zn(II)BLM-A_2. For Zn(II)PEP, additional protons in the Ala and Hist units are significantly shifted, together with Mann and Gul protons. Comparison of the significant shifts generated when all four Zn(II)BLMs bind to OL_1 indicated that just a few protons change their shifts among OL_1-bound Zn(II)BLMs. On the other hand, comparison of the $\Delta\delta$s calculated for OL_2-bound Zn(II)BLM-A_2 and Zn(II)PEP present a different picture for these two Zn(II)BLMs in terms of the chemical and/or magnetic environment their D1 protons experience. Based on these results we can propose that OL_2 has a stronger influence on the environment of D1 than OL_1. Additionally, we can see that binding to OL_2 significantly affects the shifts of the Hist moiety in Zn(II)PEP, and the disaccharide unit in Zn(II)BLM-A_2, which could be interpreted to indicate that each BLM anchor itself differently to the same DNA-binding sites.

Before binding to the OLs, D1 in the free Zn(II)BLMs displays a multitude of NOEs connecting it to the disaccharide, linker, and, in some cases, the BLM tail. This fact indicates that the Zn(II)BLMs are folded in solution. Comparison of Figures 4–6 shows that the network of NOEs displayed by D1 is greatly simplified (only a few native NOEs remain) after the Zn(II)BLMs bind to the OLs, with OL_2 causing more extensive simplification than OL_1. The remaining native and the new NOEs that arise after OL binding are different for each Zn(II)BLM (Figures 5 and 6). Additionally, comparison of the OL_1 and OL_2-bound Zn(II)BLMs indicates that the binding site in OL also has an effect on the folding of the Zn(II)BLM molecule. The Pyr and Ala moieties remain connected to each other in the

OL-bound forms of the drug, although through less NOEs than in the free forms, possibly due to their closeness in the chemical structure of the BLM molecule. On the other hand, the NOE connectivities of these moieties to the disaccharide and Hist units are more tenuous, hinting slight distortions of the metal-coordination cage that are different depending on the Zn(II)BLM and the DNA-binding site. Connections between D1 and the BLM tails are scarce in OL_1-bound forms of the drug (only observed for Zn(II)BLM-A_5), and are found in both forms of the OL_2-bound drugs. The extensive simplification of the NOE network in the OL_2-bound Zn(II)BLMs is consistent with more protons in Zn(II)BLM triads exhibiting significant shifts.

Based on the results of the investigation discussed herein, we are prone to propose that the different anchors (DNA-binding domains) used by each BLM to bind DNA, and the available DNA-binding site can produce different folding of the rest of the BLM molecule around the OLs. It is possible that the interactions of each BLM with specific DNA-binding sites could change upon binding, to arrange the MBLM molecule to achieve the best conformation for optimal DNA binding and cleavage.

Previous studies of Zn(II)BLM-A_2 and -A_5 bound to a DNA fragment of sequence $d(CGCTAGCG)_2$ [37] reported to observe more structural disturbance of the Zn(II)BLM-A_5 structure than that of Zn(II)BLM-A_2. These findings are corroborated by the results described herein. On the other hand, Vanderwall et al. investigated the deviations to the HOO-Co(III)BLM-A_2 structure when complexed with both 5′-GC-3′ and 5′-GT-3′ binding sites, and concluded that the binding site did not significantly affect the MBLM structure [38,43]. The evidence provided here shows dramatic differences of the Zn(II)BLM structure upon complexation with both binding sites. It is possible that the metal ion coordinated to the BLM could be causing the differences in the results of both investigations, and the influence of the metal center on the structure of the DNA-bound MBLM is a task worth taking.

In our series of studies on the conformational changes exhibited by OLs [50,51] and Zn(II)BLMs upon the formation of Zn(II)BLM-OL triads, we have provided molecular information on the deviations of the DNA and Zn(II)BLM structures upon triad formation with consistency and comparability. We have found that the C-termini and the DNA-binding site have an effect on the conformations of both the OL and the BLM molecule, with the 5′-GT-3′ binding site showing the most dramatic changes. At this point in our investigation, we cannot directly correlate the degree of disturbance in the Zn(II)BLM and DNA structures to the level of pulmonary toxicity produced by each of the BLMs considered. However, it is interesting that when comparing the effect of the C-substituents on the conformations of OL_1 (5′-CG-3′ binding site), Zn(II)PEP and Zn(II)BLM-A_5 produced the lowest and highest levels of disturbance to this OL, respectively. Additionally when complexed with OL_1, the shifts of the protons and the inter-residue NOE network of Zn(II)PEP were affected the least followed by Zn(II)BLM-A_2 and -B_2, with Zn(II)BLM-A_5 in order of increasing disturbance. PEP and BLM-A_5 are in the opposite ends of the toxicity spectrum of BLMs, with PEP reported to have a lower degree of pulmonary toxicity [32,34,55,56], and BLM-A_5 with a high level of toxicity [26–31]. Based on these results, it is tempting to propose a possible connection between the level of disturbance of both target and drug upon triad formation, and that of pulmonary toxicity resulting from the use of different BLMs in cancer chemotherapy. A better understanding of the molecular mechanism of MBLM-DNA complexes is necessary to advance the development of analogs of bleomycin with lower pulmonary toxicity levels and higher therapeutic activity.

4. Materials and Methods

BLM-A_2 and -B_2 were purchased from TOKU-E (Bellingham, WA, USA). BLM-A_5 was purchased from LKT Laboratories, Inc. (St. Paul, MN, USA). PEP was a generous gift from Nippon Kayaku Co., Ltd. (Tokyo, Japan). Zinc sulfate hexa-hydrate was purchased from VWR (Radnor, PA, USA). Deuterated water (99.9%, d), sodium hydroxide, and sodium chloride were purchased from Sigma-Aldrich (St. Louis, MO, USA). The oligonucleotides: 5′-AGCCTTTTGGCCT-3′

(OL_1), and 5′-CCAGTATTTTTACTGG-3′ (OL_2) used for binding to Zn(II)BLMs were purchased from Integrated DNA Technologies, Inc. (Coralville, IA, USA).

4.1. NMR Sample Preparation

BLM samples, 1.95 μmol, were dissolved in 650 μL of D_2O. A 0.12 M aqueous solution of $ZnSO_4 \cdot 7H_2O$ was mixed with the BLM solution to achieve a 1:1 molar ratio of Zn(II):BLM. The pH (meter reading uncorrected for the deuterium isotope effect) was adjusted to 6.5 with a 0.1 M NaOD solution. DNA, 0.335 μmol, was dissolved in 603 μL D_2O, and 67 μL of a 200 mM NaCl solution was added. The pH adjusted to 6.5 for the DNA samples. The Zn(II)BLM solutions were titrated with the DNA samples until a 1:1 molar ratio for the Zn(II)BLM:DNA complex was achieved. 1D ^{1}H-NMR spectra were used to monitor the changes in the complex formation. No additional changes in the 1D spectra were observed once a 1:1 molar ratio was achieved. Zn(II)BLM and DNA samples in 90% H_2O/10% D_2O (referred to as spectra in H_2O) were prepared by analogous procedures.

4.2. NMR Spectra Collection

NMR spectra were acquired at 600 MHz on a Bruker AVANCE III 600 spectrometer (Bruker BioSpin Corp, Billerica, MA, USA) with a 5.0 mm multi-nuclear broad-band observe probe. Spectra were acquired at both 278 K and 298 K for all samples, and were referenced to HDO and H_2O as internal standards. Two-dimensional experiments including correlation spectroscopy (COSY), totally correlated spectroscopy (TOCSY) and nuclear Overhauser effect spectroscopy (NOESY) were acquired utilizing solvent suppression achieved by excitation sculpting with gradients. The mixing times for the experiments were as follows: TOCSY 40 ms, and NOESY 200 ms. The spectral width was set to 10 ppm for D_2O samples and 20 ppm for H_2O samples in both dimensions, and 512 t_1 points were acquired with 2048 complex points for each free induction decay (FID). The number of scans for t_1 point for the experiments were as follows: 48 for COSY, 32 for TOCSY, and 48 for NOESY. All spectra were Fourier transformed using Lorentzian-to-Gaussian weighting and phase-shifted sine-bell window functions. NMR spectra were processed and analyzed using Topspin3.0 (Bruker BioSpin Corp., Billerica, MA, USA) and NMR ViewJ software (One Moon Scientific, Inc., Westfield, NJ, USA).

5. Conclusions

We have examined the structural changes of Zn(II)BLM-A_2, -A_5, -B_2, and Zn(II)PEP upon complexation with DNA hairpins of sequences 5′-AGGCCTTTTGGCCT-3′ and 5′-CCAGTATTTTT ACTGG-3′. The information here complements the findings we have presented on) how both the BLM C-termini and DNA binding site cause diverse conformational changes to the same DNA hairpins upon complexation with Zn(II)BLMs. These studies provide consistency and comparability missing in the field of BLM research. We have found that after Zn(II)BLM-DNA triad formation, not only is the DNA structure diversely affected, but the BLM structure is also disturbed, possibly to accommodate to that of the corresponding OL. When comparing the effect of different Zn(II)BLMs bound to the same OL, we found that the C-termini has an effect on both the shifting of protons in the OL and Zn(II)BLM, and the network of native NOEs present in each molecule. Additionally, binding of the same Zn(II)BLMs to OL_2 (5′-GT-3′ binding site) indicates that the binding site in DNA has an effect on the conformations of the OL and BLM molecules.

The work presented herein and that discussed in our studies of the conformation of MBLM-DNA triads containing the 5′-GC-3′ and 5′-GT-3′ binding sites [50,51] will be used as the diamagnetic analogs in future studies to be performed in our laboratory to investigate the structural changes to both the DNA hairpins and Fe(II)BLM. The mentioned studies have to goal of probing the effect of the metal center in MBLM-DNA interactions. Extensive detailed research on the mode of binding of MBLMs to DNA will hopefully provide direction for designing studies to result in correlations between pulmonary toxicity and the MBLM-DNA interaction.

Supplementary Materials: The following are available online at www.mdpi.com/2312-7481/4/1/0004/s1, Figure S1: NOESY spectra for both free Zn(II)BLM-A_2 and Zn(II)BLM-A_2 bound to each of the DNA strands under study, Figure S2: NOESY spectra for both free Zn(II)PEP and Zn(II)PEP bound to each of the OLs under study, Figure S3: NOESY spectra for both free Zn(II)BLM-B_2 and Zn(II)BLM-B_2 bound to each of the OLs under study, Figure S4: NOESY spectra for both free Zn(II)BLM-A_5 and Zn(II)BLM-A_5 bound to each of the DNA strands under study, Table S1: Chemical shifts for the bleomycin residues for each of the free Zn(II)BLMs under study, Table S2: Inter-residue intramolecular NOEs for free Zn(II)BLM-A_2 and Zn(II)BLM-A_2 bound to both OLs, Table S3: Intra-residue intramolecular NOEs for free Zn(II)BLM-A_2 and Zn(II)BLM-A_2 bound to both OLs, Table S4: Inter-residue intramolecular NOEs for free Zn(II)PEP and Zn(II)PEP bound to both OLs, Table S5: Intra-residue intramolecular NOEs for free Zn(II)PEP and Zn(II)PEP bound to both OLs, Table S6: Inter-residue intramolecular NOEs for free Zn(II)BLM-B_2 and Zn(II)BLM-B_2 bound to OL_1, Table S7: Intra-residue intramolecular NOEs for free Zn(II)BLM-B_2 and Zn(II)BLM-B_2 bound to OL_1, Table S8: Inter-residue intramolecular NOEs for free Zn(II)BLM-A_5 and Zn(II)BLM-A_5 bound to OL_1, Table S9: Intra-residue intramolecular NOEs for free Zn(II)BLM-A_5 and Zn(II)BLM-A_5 bound to OL_1.

Acknowledgments: This work was supported in whole by the National Institute of Health [Grant 1R15GM106285-01A1]. Our gratitude also goes to Nippon Kayaku Co., Ltd. (Tokyo, Japan) for the generous gift of peplomycin. We also acknowledge Alexander Goroncy for help collecting the NMR data presented in this work.

Author Contributions: S.E.F. prepared the NMR samples, collected NMR data, analyzed and interpreted NMR spectra and participated on the writing of this manuscript, S.A.M., A.D.I., and T.M.R. participated in sample preparation and NMR data collection, and they also analyzed and interpreted NMR spectra, T.E.L. provided the research idea, supervised and managed the project, and participated in data interpretation and manuscript writing.

Conflicts of Interest: The authors declare no conflict of interest.

References

1. Blum, R.H.; Carter, S.K.; Agre, K. A clinical review of bleomycin—A new antineoplastic agent. *Cancer* **1973**, *31*, 903–914. [CrossRef]
2. Akiyama, Y.; Ma, Q.; Edgar, E.; Laikhter, A.; Hecht, S.M. Identification of Strong DNA Binding Motifs for Bleomycin. *J. Am. Chem. Soc.* **2008**, *130*, 9650–9651. [CrossRef] [PubMed]
3. Giroux, R.A.; Hecht, S.M. Characterization of Bleomycin Cleavage Sites in Strongly Bound Hairpin DNAs. *J. Am. Chem. Soc.* **2010**, *132*, 16987–16996. [CrossRef] [PubMed]
4. Yu, Z.; Schmaltz, R.M.; Bozeman, T.C.; Paul, R.; Rishel, M.J.; Tsosie, K.S.; Hecht, S.M. Selective Tumor Cell Targeting by the Disaccharide Moiety of Bleomycin. *J. Am. Chem. Soc.* **2013**, *135*, 2883–2886. [CrossRef] [PubMed]
5. Boger, D.L.; Cai, H. Bleomycin: Synthetic and Mechanistic Studies. *Angew. Chem. Int. Ed.* **1999**, *38*, 448–476. [CrossRef]
6. Carter, B.J.; Murty, V.S.; Reddy, K.S.; Wang, S.N. A Role for the Metal-Binding Domain in Determining the DNA-Sequence Selectivity of Fe-Bleomycin. *J. Biol. Chem.* **1990**, *265*, 4193–4196. [PubMed]
7. Kane, S.A.; Hecht, S.M. *Progress in Nucleic Acid Research and Molecular Biology*; Waldo, E.C., Kivie, M., Eds.; Academic Press: Walttham, MA, USA, 1994; pp. 313–352.
8. Hecht, S.M. The Chemistry of Activated Bleomycin. *Acc. Chem. Res.* **1986**, *19*, 383–391. [CrossRef]
9. Stubbe, J.; Kozarich, J.W. Mechanisms of Bleomycin-Induced DNA-Degradation. *Chem. Rev.* **1987**, *87*, 1107–1136. [CrossRef]
10. Povirk, L.F.; Hogan, M.; Dattagupta, N. Binding of Bleomycin to DNA—Intercalation of the Bithiazole Rings. *Biochemistry* **1979**, *18*, 96–101. [CrossRef] [PubMed]
11. Hecht, S.M. RNA degradation by bleomycin, a naturally-occurring bioconjugate. *Bioconjug. Chem.* **1994**, *5*, 513–526. [CrossRef] [PubMed]
12. Zuber, G.; Quada, J.C.; Hecht, S.M. Sequence Selective Cleavage of A DNA Octanucleotide by Chlorinated Bithiazoles and Bleomycins. *J. Am. Chem. Soc.* **1998**, *120*, 9368–9369. [CrossRef]
13. Loeb, K.E.; Zaleski, J.M.; Hess, C.D.; Hecht, S.M.; Solomon, E.I. Spectroscopic Investigation of the Metal Ligation and Reactivity of the Ferrous Active Sites of Bleomycin and Bleomycin Derivatives. *J. Am. Chem. Soc.* **1998**, *120*, 1249–1259. [CrossRef]
14. Lehmann, T.E. Molecular Modeling of the Three-Dimensional Structure of Fe(II)-Bleomycin: Are the Co(II) and Fe(II) Adducts Isostructural? *J. Biol. Inorg. Chem.* **2002**, *7*, 305–312. [CrossRef] [PubMed]

15. Lehmann, T.E.; Serrano, M.L.; Que, L., Jr. Coordination Chemistry of Co(II)-Bleomycin: Its Investigation Through NMR and Molecular Dynamics. *Biochemistry* **2000**, *39*, 3886–3898. [CrossRef] [PubMed]
16. Akkerman, M.A.J.; Neijman, E.W.J.F.; Wijmenga, S.S.; Hilbers, C.W.; Bermel, W. Studies of the Solution Structure of the Bleomycin-A2 Iron(II) Carbon-Monoxide Complex by Means of 2-Dimensional NMR-Spectroscopy and Distance Geometry Calculations. *J. Am. Chem. Soc.* **1990**, *112*, 7462–7474. [CrossRef]
17. Akkerman, M.A.J.; Haasnoot, C.A.G.; Pandit, U.K.; Hilbers, C.W. Complete Assignment of the ^{13}C-NMR Spectra of Bleomycin-A2 and its Zinc Complex by Means of Two-Dimensional NMR-Spectroscopy. *Magn. Reson. Chem.* **1988**, *26*, 793–802. [CrossRef]
18. Akkerman, M.A.J.; Haasnoot, C.A.G.; Hilbers, C.W. Studies of the Solution Structure of the Bleomycin-A2 Zinc Complex by Means of Two-Dimensional NMR-Spectroscopy and Distance Geometry Calculations. *Eur. J. Biochem.* **1988**, *173*, 211–225. [CrossRef] [PubMed]
19. Oppenheimer, N.J.; Rodriguez, L.O.; Hecht, S.M. Structural Studies of Active Complex of Bleomycin—Assignment of Ligands to the Ferrous Ion in a Ferrous-Bleomycin Carbon Monoxide Complex. *Proc. Natl. Acad. Sci. USA* **1979**, *76*, 5616–5620. [CrossRef] [PubMed]
20. Lehmann, T.E.; Ming, L.J.; Rosen, M.E.; Que, L., Jr. NMR Studies of the Paramagnetic Complex Fe(II)-Bleomycin. *Biochemistry* **1997**, *36*, 2807–2816. [CrossRef] [PubMed]
21. Lehmann, T.E.; Li, Y. Possible Structural Role of the Disaccharide Unit in Fe-Bleomycin before and after Oxygen Activation. *J. Antibiot.* **2012**, *65*, 25–33. [CrossRef] [PubMed]
22. Lehmann, T.E.; Li, Y. Solution Structure of Fe(II)-Azide-Bleomycin Derived from NMR Data: Transition from Fe(II)-Bleomycin to Fe(II)-Azide-Bleomycin as Derived from NMR Data and Structural Calculations. *J. Biol. Inorg. Chem.* **2012**, *17*, 761–771. [CrossRef] [PubMed]
23. Li, Y.; Lehmann, T.E. Coordination Chemistry and Solution Structure of Fe(II)-Peplomycin. Two Possible Coordination Geometries. *J. Inorg. Biochem.* **2012**, *111*, 50–58. [CrossRef] [PubMed]
24. Lehmann, T.E.; Topchiy, E. Contributions of NMR to the Understanding of the Coordination Chemistry and DNA Interactions of Metallo-Bleomycins. *Molecules* **2013**, *18*, 9253–9277. [CrossRef] [PubMed]
25. Schroeder, B.R.; Ghare, M.I.; Bhattacharya, C.; Paul, R.; Yu, Z.Q.; Zaleski, P.A.; Bozeman, T.C.; Rishel, M.J.; Hecht, S.M. The Disaccharide Moiety of Bleomycin Facilitates Uptake by Cancer Cells. *J. Am. Chem. Soc.* **2014**, *136*, 13641–13656. [CrossRef] [PubMed]
26. Raisfeld, I.H. Pulmonary Toxicity of Bleomycin Analogs. *Toxicol. Appl. Pharmacol.* **1980**, *56*, 326–336. [CrossRef]
27. Raisfeld, I.H.; Chovan, J.P.; Frost, S. Bleomycin Pulmonary Toxicity—Production of Fibrosis by Bithiazole-Terminal Amine and Terminal Amine Moieties of Bleomycin-A2. *Life Sci.* **1982**, *30*, 1391–1398. [CrossRef]
28. Raisfeld, I.H.; Chu, P.; Hart, N.K.; Lane, A. A Comparison of the Pulmonary Toxicity Produced by Metal-Free and Copper-Complexed Analogs of Bleomycin and Phleomycin. *Toxicol. Appl. Pharmacol.* **1982**, *63*, 351–362. [CrossRef]
29. Raisfeld, I.H. Relation between Bleomycin Structure and Pulmonary Fibrosis. *Clin. Pharmacol. Ther.* **1981**, *29*, 274.
30. Raisfeld, I.H. Relation of Bleomycin Structure to Pulmonary Toxicity. *Clin. Res.* **1980**, *28*, A530.
31. Raisfeld, I.H. Bleomycin Terminal Groups Produce Pulmonary Fibrosis. *Clin. Res.* **1979**, *27*, A445.
32. Oka, S. A Review of Clinical-Studies of Pepleomycin. *Recent Results Cancer Res.* **1980**, *74*, 163–171. [PubMed]
33. Umezawa, H. Recent Studies on Bleomycin. *Lloydia* **1977**, *40*, 67–81.
34. Tanaka, W.; Takita, T. Pepleomycin—2nd Generation Bleomycin Chemically Derived From Bleomycin A2. *Heterocycles* **1979**, *13*, 469–476. [CrossRef]
35. Sucheck, S.J.; Ellena, J.F.; Hecht, S.M. Characterization of Zn(II) Deglycobleomycin A2 and Interaction with d(CGCTAGCG)2: Direct Evidence for Minor Groove Binding of the Bithiazole Moiety. *J. Am. Chem. Soc.* **1998**, *120*, 7450–7460. [CrossRef]
36. Keck, M.V.; Manderville, R.A.; Hecht, S.M. Chemical and Structural Characterization of the Interaction of Bleomycin A2 with d(CGCGAATTCGCG)(2). Efficient, Double-Strand DNA Cleavage Accessible without Structural Reorganization. *J. Am. Chem. Soc.* **2001**, *123*, 8690–8700. [CrossRef] [PubMed]
37. Manderville, R.A.; Ellena, J.F.; Hecht, S.M. Interaction of Zn(II)-Bleomycin With d(CGCTAGCG)2—A Binding Model-Based on NMR Experiments and Restrained Molecular-Dynamics Calculations. *J. Am. Chem. Soc.* **1995**, *117*, 7891–7903. [CrossRef]

38. Vanderwall, D.E.; Lui, S.M.; Wu, W.; Turner, C.J.; Kozarich, J.W.; Stubbe, J. A Model of the Structure of HOO-CoBleomycin Bound to d(CCAGTACTGG): Recognition at the d(GpT) Site and Implications for Double-Stranded DNA Cleavage. *Chem. Biol.* **1997**, *4*, 373–387. [CrossRef]
39. Wu, W.; Vanderwall, D.E.; Lui, S.M.; Tang, X.J.; Turner, C.J.; Kozarich, J.W.; Stubbe, J. Studies of CoBleomycin A2 Green: Its Detailed Structural Characterization by NMR and Molecular Modeling and its Sequence-Specific Interaction with DNA Oligonucleotides. *J. Am. Chem. Soc.* **1996**, *118*, 1268–1280. [CrossRef]
40. Wu, W.; Vanderwall, D.E.; Stubbe, J.; Kozarich, J.W.; Turner, C.J. Interaction of CoBleomycin A2 (Green) with d(CCAGGCCTGG)2—Evidence for Intercalation Using 2D NMR. *J. Am. Chem. Soc.* **1994**, *116*, 10843–10844. [CrossRef]
41. Wu, W.; Vanderwall, D.E.; Teramoto, S.; Lui, S.M.; Hoehn, S.T.; Tang, X.J.; Turner, C.J.; Boger, D.L.; Kozarich, J.W.; Stubbe, J. NMR Studies of Codeglycobleomycin A2 Green and its Complex with d(CCAGGCCTGG). *J. Am. Chem. Soc.* **1998**, *120*, 2239–2250. [CrossRef]
42. Wu, W.; Vanderwall, D.E.; Turner, C.J.; Hoehn, S.; Chen, J.Y.; Kozarich, J.W.; Stubbe, J. Solution Structure of the Hydroperoxide of Co(III) Phleomycin Complexed With d(CCAGGCCTGG)2: Evidence for Binding by Partial Intercalation. *Nucleic Acids Res.* **2002**, *30*, 4881–4891. [CrossRef] [PubMed]
43. Wu, W.; Vanderwall, D.E.; Turner, C.J.; Kozarich, J.W.; Stubbe, J. Solution Structure of CoBleomycin A2 Green Complexed With d(CCAGGCCTGG). *J. Am. Chem. Soc.* **1996**, *118*, 1281–1294. [CrossRef]
44. Zhao, C.Q.; Xia, C.W.; Mao, Q.K.; Forsterling, H.; DeRose, E.; Antholine, W.E.; Subczynski, W.K.; Petering, D.H. Structures of HO2-Co(III)Bleomycin A2 Bound to d(GAGCTC)2 and d(GGAAGCTTCC)2): Structure-Reactivity Relationships of Co and Fe Bleomycins. *J. Inorg. Biochem.* **2002**, *91*, 259–268. [CrossRef]
45. Kuwahara, J.; Sugiura, Y. Sequence-Specific Recognition and Cleavage of DNA by Metallobleomycin—Minor Groove Binding and Possible Interaction Mode. *Proc. Natl. Acad. Sci. USA* **1988**, *85*, 2459–2463. [CrossRef] [PubMed]
46. Goodwin, K.D.; Lewis, M.A.; Long, E.C.; Georgiadis, M.M. Crystal Structure of DNA-Bound Co(III)-Bleomycin B-2: Insights on Intercalation and Minor Groove Binding. *Proc. Natl. Acad. Sci. USA* **2008**, *105*, 5052–5056. [CrossRef] [PubMed]
47. Lui, S.M.; Vanderwall, D.E.; Wu, W.; Tang, X.J.; Turner, C.J.; Kozarich, J.W.; Stubbe, J. Structural Characterization of CoBleomycin A2 Brown: Free and Bound to d(CCAGGCCTGG). *J. Am. Chem. Soc.* **1997**, *119*, 9603–9613. [CrossRef]
48. Caceres-Cortes, J.; Sugiyama, H.; Ikudome, K.; Saito, I.; Wang, A.H.J. Interactions of Deglycosylated Cobalt(III)—Pepleomycin (Green Form) with DNA Based on NMR Structural Studies. *Biochemistry* **1997**, *36*, 9995–10005. [CrossRef] [PubMed]
49. Caceres-Cortes, J.; Sugiyama, H.; Ikudome, K.; Saito, I.; Wang, A.H.J. *Structure, Motion, Interaction and Expression of Biological Macromolecules*; Sarma, R.H., Sarma, M.H., Eds.; Adenine Press: New York, NY, USA, 1998; pp. 207–225.
50. Lehmann, T.E.; Murray, S.A.; Ingersoll, A.D.; Reilly, T.M.; Follett, S.E.; Macartney, K.E.; Harpster, M.H. NMR Study of the Effects of Some Bleomycin C-Termini on the Structure af a DNA Hairpin With the 5′-GC-3′ Binding Site. *J. Biol. Inorg. Chem.* **2017**, *22*, 121–136. [CrossRef] [PubMed]
51. Follett, S.E.; Ingersoll, A.D.; Murray, S.A.; Reilly, T.M.; Lehmann, T.E. Interaction of Zn(II)Bleomycin-A2 and Zn(II)Peplomycin With a DNA Hairpin Containing the 5′-GT-3′ Binding Site in Comparison with the 5′-GC-3′ Binding Site Studied by NMR Spectroscopy. *J. Biol. Inorg. Chem.* **2017**, *22*, 1039–1054. [CrossRef] [PubMed]
52. Ohno, M.; Otsuka, M. *Recent Progress in the Chemical Synthesis of Antibiotics*; Lukacs, G., Ohno, M., Eds.; Springer: Berlin, Germany, 1990; pp. 387–414.
53. Glickson, J.D.; Pillai, R.P.; Sakai, T.T. Proton NMR-Studies of the Zn(II)-Bleomycin-A2-Poly(dA-dT) Ternary Complex. *Proc. Natl. Acad. Sci. USA* **1981**, *78*, 2967–2971. [CrossRef] [PubMed]
54. Xu, R.X.; Nettesheim, D.; Otvos, J.D.; Petering, D.H. NMR Determination of the Structures of Peroxycobalt(III) Bleomycin and Cobalt(III) Bleomycin, Products of the Aerobic Oxidation of Cobalt(II) Bleomycin by Dioxygen. *Biochemistry* **1994**, *33*, 907–916. [CrossRef] [PubMed]

55. Raisfeld, I.H.; Kundahl, E.R.; Sawey, M.J.; Chovan, J.P.; Depasquale, J. Selective Toxicity of Specific Lung-Cells to Bleomycin. *Clin. Res.* **1982**, *30*, A437.
56. Takahashi, K.; Aoyagi, H.S.; Koyu, A.; Kuramochi, H.; Yoshioka, O.; Matsuda, A.; Fujii, A.; Umezawa, H. Biological Studies on the Degradation Products of 3-[(S)-1′-Phenylethylamino]Propylaminobleomycin—Novel Analog (Pepleomycin). *J. Antibiot.* **1979**, *32*, 36–42. [CrossRef] [PubMed]